Low-cost Ca-based composites synthesized by biotemplate method for Thermochemical Energy Storage of Concentrated Solar Power

Monica Benitez-Guerrero [1, 2], Jose Manuel Valverde [1], Antonio Perejon [2, 3], Pedro E. Sanchez-Jimenez [2], Luis A. Perez-Maqueda [2].*

[1] Facultad de Física, Universidad de Sevilla, Avenida Reina Mercedes s/n, 41012 Sevilla, Spain.

[2] Instituto de Ciencia de Materiales de Sevilla, C.S.I.C.-Universidad de Sevilla, C. Américo Vespucio nº49, 41092 Sevilla, Spain.

[3] Facultad de Química, Universidad de Sevilla, Avenida Reina Mercedes s/n, 41012 Sevilla Spain.

*Prof. Dr. J.M. Valverde

Facultad de Física

Universidad de Sevilla

Avenida Reina Mercedes s/n, 41012 Sevilla (Spain)

Tel +34 954550960 Fax +34 954239434

E-mail: jmillan@us.es

Low-cost Ca-based composites synthesized by biotemplate method for thermochemical energy storage of concentrated solar power

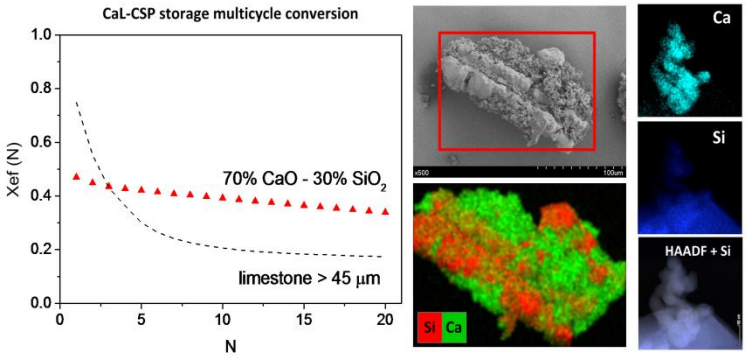

Highlights

***** CaO/SiO_2 composites were synthesized by a low cost biomimetic process from rice husk

***** CaO/SiO_2 composites are highly efficient for concentrated solar energy storage

*The composites show significantly better performance than natural limestone

*****Pore-plugging is reduced by the composition and microstructure of the CaO/SiO_2 composites

Abstract

An ever more environmentally conscious society demands the use of green, sustainable and high-efficiency renewable energy resources. However, large-scale energy storage remains a challenge for a deep penetration of power produced from renewables into the grid. The Calcium-Looping (CaL) process, based on the reversible carbonation/calcination of CaO, is a promising technology for thermochemical energy storage (TCES) in Concentrated Solar Power (CSP) plants. Natural limestone to be used as CaO precursor is cheap, non-toxic and abundant. Nevertheless, recent works have shown that carbonation of CaO derived limestone at optimum conditions for TCES is limited by pore-plugging, which leads to severe deactivation for large enough particles to be employed in practice. In our work, we have synthesized inexpensive CaO/SiO_2 composites by means of a biotemplate method using rice husk as support. The morphological and compositional features of the biomorphic materials synthesized help improve the CaO multicycle activity under optimum CSP storage conditions and for particles sufficiently large to be managed in practical processes.

Keywords: Renewable resources; Energy conversion; Thermochemical Energy storage; Calcium Looping; Biomorphic composites.

1. Introduction

The Calcium-Looping (CaL) process based on the reversible carbonation/calcination reaction of CaO:

$$CaO_{(s)} + CO_{2(g)} \rightleftarrows CaCO_{3(s)} + \Delta H_r^0 \quad ; \qquad \Delta H_r^0 = 178\ kJmol^{-1} \tag{1}$$

has been extensively studied in the last years to capture CO_2 from fossil fuel-fired power plants [1-3] as originally proposed by Shimizu et al. [4]. In the late 1970s the CaL process was early investigated for thermochemical energy storage (TCES) of concentrated solar power (CSP) [5, 6]. In the last years most of the works on energy storage in CSP has been focused on molten salts technology [7-10] and redox-based systems [11-13]. The use of the CaL process to this end has not attracted a wide interest until quite recently as it would allow long term storage of massive amounts of energy at low cost and using abundant and non-toxic materials such as limestone [14]. A flow diagram of the integration of the CaL process in CSP plants recently proposed elsewhere [14] built upon a closed CO_2 cycle is shown in Fig. 1. It basically consists of a solar calciner, a carbonation reactor, a CO_2 compression-storage system, two reservoirs for CaO and $CaCO_3$ storage and a power unit. After calcination of $CaCO_3$ in the calciner using concentrated solar energy, the sensible heat of CaO and CO_2 is recovered and these products are stored independently. On demand, CaO and CO_2 are circulated into the carbonator wherein heat is released by the exothermic carbonation reaction. This heat is transported by the CO_2 in excess to a gas turbine where electricity is generated while the effluent CO_2 is sent to storage.

Optimum CaL conditions to obtain the maximum overall efficiency from the CaL-CSP integration involve high temperature carbonation (above 850 ºC) under high CO_2 concentration. Remarkably, these conditions differ from those corresponding for CO_2 capture in which calcination is carried out under high CO_2 concentration at high temperature (above 900 ºC) and carbonation occurs at relatively lower temperature (around 650 ºC) under low CO_2 concentration (around 15% vol.) [14]. Among calcium oxide based sorbents, natural limestone (nearly 100% $CaCO_3$) the most preferable CaO precursors since it is environmentally friendly, inexpensive,

abundant and widely available [15]. However, a major challenge to use limestone is the severe loss of activity of the regenerated CaO after just a few cycles of carbonation/decarbonation. Deactivation at CaL-CO_2 capture conditions is due to the marked sintering suffered by the CaO grains under the necessary harsh calcination conditions, which involve high temperatures and high CO_2 partial pressure [16]. On the other hand, pore-plugging is a critical limiting mechanism at CaL-CSP storage conditions as carbonation at high temperature and under high temperature is very fast, which makes it likely that the thick $CaCO_3$ layer blocks the inner pores of the CaO particles [17, 18].

In order to avoid deactivation, the use of different additives such as Al_2O_3, La_2O_3, Li_2CO_3, MgO, SiO_2, TiO_2, Y_2O_3 and ZrO_2 has been investigated in previous works [19-25]. These studies have been mostly focused on the use of the CaL process for CO_2 capture [2, 3, 15]. Taking into account the large scale of the application (typically around 500 tons of raw limestone would be needed in the CaL process to capture the CO_2 released from a commercial coal fired power plant) [26], a compromise between sorbent cost production and its multicycle activity performance is required [27]. Thus, silica is a promising additive as it is not expensive and a wide spread reliable inert material. Nanostructured silica, both in the form of molecular sieves [28] and nanoparticles [29] serves to improve the dispersibility of CaO agglomerates [29] and mitigate sintering [30], which is attributed to the formation of calcium silicates at high temperatures that confer thermal stability to the CaO skeleton at the harsh calcination conditions used for CO_2 capture [31]. Nonetheless, the synthesis of nanostructured silica from either sol-gel routes or flame synthesis, which is employed in commercially available products such as Aerosil®, has a high cost. In contrast, the use of rice husk biomass (a by-product of rice husk industry), as proposed in the present work, is an alternative cost-effective method to produce nanosilica at massive amounts. Hence, rice husk ash has been used as additive to synthesize CaO sorbents for CO_2 capture [32, 33]. In this sense, several works have been reported on the use of raw rice husk to generate porous CaO pellets for CO_2 capture with improved CO_2 sorption performance [34, 35].

However, the effect of silica in SiO_2/CaO mixtures on the activity of CaO cycled at CaL conditions for CSP storage remains largely unexplored yet. Recently, the CaL-CSP multicycle performance of a nano-SiO_2/CaO composite derived by physical mixing of a commercial SiO_2 nanopowder and limestone was analyzed by our group [17]. Quite surprisingly, it was found that the presence of nanosilica caused a significant deterioration of the multicycle CaO activity, in contrast with previous results obtained at CaL conditions for CO_2 capture [30]. The action of nanosilica, by shifting the CaO mesoporous size distribution to smaller pore sizes, was found to hinder CaO carbonation by promoting pore-plugging, which is the main limiting factor on CaO conversion at CaL conditions for CSP storage.

In the present work, rice husk has been employed to synthesize CaO/SiO_2 composites by a biotemplate route to generate a microstructural porosity in CaO, while at the same time the composites reproduce the micro and nanostructure of the husk. To the best of our knowledge, no further studies have described the use of such kind of composites for thermochemical energy storage of CSP. The multicycle performance of the CaO/SiO_2 composites synthesized in this way is significantly improved as compared to limestone at CaL-CSP conditions. These results are significantly important as they are obtained for particles of size large enough to be used in the practical application in circulating fluidized bed reactors.

2. Experimental Section

2.1. Chemicals and Materials

$Ca(NO_3)_2 \cdot 4H_2O$ (Sigma-Aldrich) and raw rice husk (Herba Ricemills S.L.) were used in our work to synthesize CaO/SiO_2 composites. Natural limestone (>99 %wt $CaCO_3$) from Matagallar quarry in Pedrera (Sevilla, Spain) was also used for the sake of comparison. Two size fractions of this limestone (less than 45 μm and 45-160 μm) were employed (Fig.A1 in Appendix A, Supplementary Content).

2.2. Synthesis of CaO/SiO_2 composites

Raw rice husk was pretreated to be used as biotemplate as detailed in Appendix A in order to obtain high purity nanostructured SiO_2 of large specific surface area. For this purpose 0.1L $Ca(NO_3)_2 \cdot 4H_2O$ solutions of 0.5 and 2 M were prepared for the infiltration of 10 g of as-pretreated rice husk. The infiltrating solutions and the pretreated rice husk were maintained at 50 ºC during 24 h under stirring, until infiltration and water evaporation were achieved. Finally, the products were oven-dried at 120 ºC before thermal treatment. The two steps thermal treatment was conducted at the same conditions detailed in the Appendix for the ash synthesis. The nominal compositions of the biotemplated composites are 30wt%SiO_2/70wt%CaO and 10wt%SiO_2/90wt%CaO (labeled hereafter as 70%CaO and 90%CaO, respectively).

2.3. Material Characterization

Compositional analysis was carried out by X-ray fluorescence (XRF) using an Axios PW4400 (PANalytical) instrument and energy-dispersion X-ray (EDX) using a Bruker-X Flash-4010 detector. Powder X-ray diffraction (XRD) was performed using a MiniFlex600 (Rigaku) operated with Ni filtered CuKα radiation (λ = 1.5406 Å) at 40 kV and 15 mA for a scan range 2θ=5–90° at a step rate of 5° min^{-1}.

Particle size distributions (PSDs) were obtained by laser diffractometry using a Mastersizer 2000 (Malvern). To this end, the samples were previously dispersed in 2-propanol (as recommended for Ca-based materials according to ISO 14887 [36]) and sonicated for 30 s to loose particle agglomerates.

Nitrogen adsorption-desorption isotherms at 77 K were acquired by means of a TriStar II 3020 (Micromeritics) instrument. The samples were degassed at 150 ºC for 2 h. Specific surface area (S_{BET}) was calculated using the BET equation [37]. Total pore volume (Vsp) was determined from the amount of gas adsorbed at a P/P_0 value of 0.97. Mesopore distributions were derived by the BJH method applied to the adsorption branch of the isotherms [38]. The average pore sizes (wp and wp_{BJH}) were determined by approximating the pore geometry to a cylinder.

Scanning Electron Microscopy (SEM) micrographs and compositional EDX mapping were acquired using a Hitachi S4800 FEG microscope on gold-sputtered samples.

Transmission Electron Microscopy (TEM) and High-angle Annular Dark-Field Scanning Transmission Electron Microscopy (HAADF-STEM) micrographs were registered using a Talos F200S FEG microscope (FEI company) in which the powder samples were deposited on copper grids.

2.4. Calcium Looping (CaL) Multicycle Conversion

CaL multicycle tests were carried out using a Q5000IR thermogravimetric analyzer (TA Instruments), which is provided with a high sensitivity balance (<0.1 μg) and a furnace heated by IR halogen lamps that allow for high heating and cooling rates (up to 300 ºC min^{-1}) to be expected under practical conditions. The samples were subjected to CaL conditions leading to high efficiency for TCES of CSP as reported elsewhere [14]. Each run was initiated with a precalcination stage under helium atmosphere from room temperature to the calcination temperature of 725 ºC, with a heating ramp of 300 ºC min^{-1}. Afterwards, the temperature was quickly (300 ºC min^{-1}) increased to 850 ºC for carbonation under pure CO_2 for 5 min. Carbonation was followed by a rapid decrease (300 ºC min^{-1}) of temperature to 725 ºC for calcination under pure He during 5 min. In order to simulate the extraction of sensible heat from the solids in a real plant before they are stored, the temperature was decreased (at 100ºC min^{-1}) to 300 ºC and kept there for 2 min under He between the carbonation and calcination stages. A total of 20 carbonation/calcination cycles were run in this way for the CaO/SiO_2 composites and natural limestone. A schematic representation of the procedure is given in Fig. A2.

Additional tests extended up to 50 cycles were carried out in order to analyze the long-term performance of the materials as well as data reproducibility. In the practical application, the material would not be cycled indefinitely. Due to the significant drop of conversion of limestone derived activity after just 20 cycles, a certain amount of material should be periodically purged while fresh limestone is fed into the system to balance out mass. The average number of cycles

that a particle undergoes in the CaL process will depend on the recirculation flow rate of solids between the carbonator and the calciner and the flow rate of fresh limestone introduced [39]. Thus, the analysis of the multicycle activity of the material along a finite number of cycles yields useful information on its performance for practical purposes.

The multicycle CaO conversion, X_{CaO}, for the CaO/SiO_2 composites is calculated as

$$X_{CaO\ N} = \frac{m_{Carb\ N} - m_N}{m_N} \cdot \frac{W_{CaO}}{W_{CO2}} \cdot \left(\frac{1}{f}\right) \quad (2)$$

where m_N and $m_{Carb\ N}$ are the sample masses before and after carbonation at the Nth-cycle and W_{CaO} and W_{CO2} are the molar masses of CaO and CO_2, respectively. In Eq 2, *f* is the fraction of CaO in the mixture. The very small amount of calcium silicates formed, as observed from XRD, is neglected. A more relevant parameter for practical purposes to assess the performance of the samples is the effective conversion, $X_{ef\ N}$, defined as the ratio of the CaO mass converted in the carbonation stage of each N-cycle to the total sample mass before carbonation

$$X_{ef\ N} = \frac{m_{Carb\ N} - m_N}{m_N} \cdot \frac{W_{CaO}}{W_{CO2}} \quad (3)$$

The use of X_{ef} takes into account the presence of inert compounds in the composites. Thus, the specific energy released in the carbonation stage per mass unit would be given by X_{ef} times ($\Delta Hr^0/W_{CaO}$) (kJ g^{-1}), where ΔHr^0 is the reaction enthalpy (-178 kJ mol^{-1}).

3. Results and Discussion

The pretreated rice husk (Appendix A), employed as biotemplate to synthesize the CaO/SiO_2 composites, is characterized by a globular external surface and the presence of inner channels (Fig. A3). After combustion of the carbonaceous material, the compositional analysis of the obtained ash reveals that Si is the main element of the rice husk ash, followed by Ca, Mg, Fe, K and Mn in minor proportions as well as other trace elements such as Na, Al, S, P (as shows Table 1). In agreement with previous studies [40-43], the main ash component generated after

thermal treatment of rice husk is nanostructured silica (SiO_2), which is mainly amorphous in our case as shown in Fig. A5a. The specific surface area of the obtained ash is significantly high, S_{BET} = 218 $m^2 g^{-1}$ as well as the corresponding pore volume, Vp = 0.35 $cm^3 g^{-1}$. The typical pore size is about 3 nm as observed in Fig. A5b. These values are similar to data reported elsewhere [40]. SEM micrographs in Fig. A6 show that the ash replicates the microstructure of rice husk with a shrinkage factor due to the loss of biomass. SEM analysis on the rice husk ash shows a porous structure in which the bulbous forms and channels observed in the raw rice husk are still clearly identified. The nanoparticles that compose the whole structure, mainly amorphous silica, have been analyzed by HRTEM. The size of these nanoparticles is around 10-40 nm, which is similar to the size of the intraparticle pores (Fig. A7).

Table 1. Compositional analysis of rice husk ash as determined from XRF (shown as oxides in weight percent).

	% Wt		**% Wt**
Al_2O_3	0.07	**Na_2O**	0.06
CaO	1.90	**NiO**	0.02
Cr_2O_3	0.09	**P_2O_5**	0.17
Fe_2O_3	0.31	**SO_3**	0.28
K_2O	0.34	**SiO_2**	95.8
MgO	0.78	**ZnO**	0.02
MnO	0.15		

For infiltration a $Ca(NO_3)_2 \cdot 4H_2O$ solution is employed to fill the pores of the biotemplate matrix up to cover completely the inner and outer surface of the pretreated rice husk. During the first step of the thermal treatment, the infiltrated mixture is heated up to 600 °C in nitrogen. Water from the inorganic salt and the cellulosic material is progressively released until about 200 °C. $Ca(NO_3)_2$ melts at 560 °C and subsequent decomposition ($2Ca(NO_3)_2 \rightarrow 2CaO + O_2 + 4NO_2$) occurs in the molten phase [44]. A mixture of the carbonaceous skeleton and inorganic material, mainly amorphous CaO and SiO_2, is produced after this stage. In a second step, combustion of

the carbonaceous material takes place at 600 ºC under air. CO_2 and H_2O generated react with the CaO particles to form $CaCO_3$ and $Ca(OH)_2$ as observed from XRD for both composites (Fig. A8). Arguably an intermediate specie Ca-(OH)* that could be formed in amorphous state could quickly react with the CO_2 from the combustion of the rice husk char to form the carbonate. The broad amorphous peak at 2θ =15-30º could be attributed to the presence of still a significant amount of amorphous SiO_2 in the composite of lower CaO content (70%CaO composite).

After thermal treatment, the synthesized inorganic composites replicate the morphology of rice husk as observed in the SEM micrographs of the composites derived with different CaO load: 70%CaO (Fig. 2 a, b) and 90%CaO (Fig. 2 c, d). The composite with smaller CaO load is characterized by a porous morphology, with $CaCO_3$ loose particles and some fragments rich in SiO_2 as obtained from the EDX analysis. On the other hand, the composite with higher CaO content presents a thicker and compact surface, showing a better replica of the template. These observations are also supported by the porosity results obtained by nitrogen adsorption-desorption isotherms (Table 2). Accordingly, the 70%CaO composite has a S_{BET} value of 25 $m^2 g^{-1}$ whereas the 90%CaO composite S_{BET} value is close to 7 $m^2 g^{-1}$. The larger pore volume of the 70%CaO composite is reflected in its BJH distribution, which peaks at 6 nm (Fig. 3a). These microstructural features are consistent with the ranges of particle size measured by laser diffractometry for both composites (PSDs are shown in Fig. 3b). Thus, a reduced agglomeration of the particles of the 70%CaO sample leads to lower particle sizes (1-100 μm) as compared to the larger compact 90%CaO composite particles (1-1000 μm).

Table 2. Porosity data measured by nitrogen adsorption-desorption analysis.

	70%CaO	**90%CaO**

S $_{BET}$ ($m^2 g^{-1}$)	25.0	6.6
Vsp ($cm^3 g^{-1}$)	0.074084	0.027219
Wp (nm)	11.8	16.3
Wp BJH (nm) Ads	17.3	25.5

HRTEM micrographs of as-prepared composites show that the average size of crystalline domains, corresponding to the main crystalline phase $CaCO_3$, is close to 5-10 nm for both composites (Fig. A9 and A10). A homogenous distribution of Ca across the particles of both composites is observed by HAADF-STEM mapping (Fig. A9 and A10) whereas the distribution of Si is determined by the own biologic nature of the parent rice husk [45], which is not directly related to the synthesis process.

Fig. 4 shows the time evolution of sample weight and temperature during the first and 20th carbonation/calcination cycles (under CaL-CSP storage conditions) carried out by TGA for the CaO/SiO_2 composites synthesized. As may be seen in Fig. 4, carbonation takes place through two well differentiated phases as widely described in the literature for CaO based sorbents [46, 47]. A first fast reaction controlled phase taking place at the surface of the CaO grains is followed by a much slower solid-state diffusion controlled phase which is limited by the counter-current diffusion of inward CO_3^{2-} anion groups and outward O^{2-} anions across the $CaCO_3$ product layer [48, 49]. As observed in previous works [18, 50], the fast reaction-controlled phase is the main contribution to the overall carbonation along all cycles under CaL-CSP storage conditions. In these CaL conditions, which involve carbonation under high CO_2 concentration and high temperature, the reaction controlled fast regime occurring at the surface of the particles is greatly promoted as compared to the solid-state diffusion controlled stage [26].

Fig. 4a shows that CaO conversion in the first carbonation stage is very similar for both composites (70% and 90%CaO). However, the composite with higher SiO_2 content (70%CaO) is carbonated to a higher level at the 20^{th} cycle (Fig. 4b). Data on the multicycle CaO conversion X_{CaO} and effective conversion X_{ef} (ratio of CaO converted to total weight of the sorbent including inert SiO_2) are plotted in Fig. 5. For comparison, data are plotted also on the multicycle conversion

measured for natural limestone derived CaO (lime) reported elsewhere [18]. Data for extended tests up to 50 cycles are shown in Fig. 6, which demonstrates data reproducibility and further confirms the slower decay of conversion for both 70%CaO and 90%CaO composites compared to limestone. After 50 cycles, the effective conversion of the 70%CaO composite is kept slightly higher than the 90%CaO composite.

In contrast with the behavior exhibited by the composites, lime conversion suffers a severe drop after just a few cycles due to pore-plugging [18]. As discussed in our previous work [18], the relatively low calcination temperature in these CaL conditions leads to a highly porous CaO skeleton which is blocked by the thick $CaCO_3$ layer quickly built upon the particle's surface during carbonation at high temperature and under high CO_2 concentration as may be inferred from the SEM pictures in Fig. 7. This micrograph of the cycled limestone sample after being subjected to the CaL cycles (ending in calcination) show a sintered CaO layer on the surface of the particles whereas inner parts becoming exposed by particle fracturing exhibit a porous CaO skeleton, which has arguably not intervened in the carbonation reaction during the cycles. In contrast with the behavior of limestone, Fig. 5 shows that higher conversion values are obtained for the CaO/SiO_2 composites with particles much larger (Fig. 3) than this critical value (~45 μm) for limestone. These results indicate that pore-plugging is not a limiting factor for carbonation of the CaO/SiO_2 composites. This may be specifically attributed to the novel synthesis method employed as previous results demonstrated that pore-plugging did hinder carbonation of CaO/SiO_2 composites prepared by physical mixing [17].

The morphology of the CaO/SiO_2 composites after being subjected to the CaL cycles is illustrated by the SEM pictures shown in Fig. 8. These SEM micrographs evidence some differences between the 70%CaO and 90%CaO cycled samples. After the 20 CaL cycles, the composite with higher SiO_2 content maintains a foamy surface structure, with small pores and visible SiO_2 plates (Fig. 8a and Fig. 9). On the contrary, the surface of the 90%CaO composite is apparently more compact with relatively larger pores of several tens microns size. Arguably, the porous structure of the 70%CaO composite and the deep cavities formed between the SiO_2 plates

and CaO grains would facilitate the diffusion of CO_2 into the inner pores during carbonation, thus circumventing pore-plugging. This characteristic morphological structure would lead to a better multicycle performance of the composite with the lower CaO content. In addition, the compositional mapping reveals that Si is present not only on the external surface (Fig. 9) but also in the inner walls that mimic rice husk as observed in Fig. A11 (Appendix). The higher CaO load of the 90%CaO composite and the limited EDX resolution could explain why silicon is hidden in the corresponding compositional mapping (Fig. A12). Nonetheless, the distribution of SiO_2 in the grains at the nanoscopic level for both composites is demonstrated by the HAADF-STEM compositional images (Fig. 10 and Fig. A13).

HRTEM micrographs (Fig. 10 and Fig. A13) of the samples after being cycled show the presence of wide crystalline domains, which can be attributed to the main $CaCO_3$ and CaO phases. SiO_2 is maintained in an amorphous phase after 20 cycles for both composites (no crystalline SiO_2 phase has been detected by XRD). In addition to $CaCO_3$ and CaO, the formation of calcium silicate ($CaSiO_3$) and calcium orthosilicate (Ca_2SiO_4) has been detected by XRD although just by a small amount as inferred from the rather small intensity of their reflection peaks (Fig. 11). The thermally stable and well distributed amorphous silica and the formation of these silicate compounds would serve also to counteract grain sintering due to their high melting point.

In brief, the importance of the work here presented lies mostly on the simplicity of manufacture of CaO/SiO_2 composites with an acceptable multicycle stability under the CaL-CSP storage conditions analyzed, comprising finely dispersed inert phase and particle sizes useful for practical applications in circulating fluidized beds.

Since the final purpose of the composites synthesized is to store energy it is relevant to estimate the energy density of these composites and to compare it with that of the $CaCO_3$/CaO system in order to assess the suitability of these materials in solar plants. A definition of gravimetric energy density, D_m (MJ kg^{-1}) is given by Pardo et al. [51], expressed as

$$D_m = \frac{Q}{\sum m_{out}} \quad (4)$$

Where Q is the stored thermal energy (MJ) and $\sum m_{out}$ is the total material mass (kg) leaving the calciner, that is, the calcination products (CaO, CO_2 and the inert material, SiO_2 in our case) from which the chemical and calorific energy will be released when needed. D_m can be thus calculated as the sum of the calcination entalphy and the sensible heat required to raise the temperature of the material entering to the calciner from room temperature to the reaction temperature (calcination temperature):

$$D_m = \frac{m_{in}\Delta H_r + \sum_i m_i \int_{Tin}^{Tcal} C_{p,i} dT}{\sum m_{out}} \quad (5)$$

where m_{in} is the reactive material mass at the entrance of the calciner (kg), i.e. $CaCO_3$, ΔH_r is the reaction enthalpy (MJ kg^{-1}), $C_{p,i}$ is the specific heat of each component (MJ kg^{-1} K^{-1}), that is, $CaCO_3$, inert material (SiO_2), and unreacted CaO if any. T_{cal} is the calcination temperature and T_{in} the temperature of the solids entering to the calciner. Thus, from Eq. (5), the gravimetric energy densities can be inferred knowing the mass fraction of inert material (%SiO_2) and reactive material (%$CaCO_3$) in the synthetized composites, the variation of Cp with temperature for $CaCO_3$ and SiO_2 between the inlet and calcination temperatures for the first cycle (25 and 725 ºC) [52]. The results of the calculations yield D_m values of 2.55, 2.44 and 2.20 MJ kg^{-1} for pure $CaCO_3$, 90%CaO/10%SiO_2 and 70%CaO/30%SiO_2 composites, respectively. A fraction of SiO_2 of 6%wt in the reactive carbonate leads to a reduction by 4% of the D_m value, whereas the presence of 19%wt of SiO_2 yields a reduction close to 13%. Note that the slight variation of Cp with temperature does not influence notably the values of energy density in the low temperature range. Thus, for the subsequent cycles carried out using 300 ºC as inlet temperature in the intermediate stage (in order to simulate the extraction of sensible heat of solids) and 725 ºC as calcination temperature, the energy density values can be estimated as 2.28, 2.17 and 1.94 for $CaCO_3$, 90%CaO and 70%CaO samples, respectively. However, the higher effective conversion and multicycle stability of theses composites compared to the limestone with equivalent particle sizes, could compensate a lower energy density. From a techno-economic point of view these results

should be considered for further research to analyze in depth the advantages of using this kind of CaO/SiO_2 composites in practice.

4. Conclusions

This work reports the synthesis of porous CaO/SiO_2 composites by biotemplate route using rice husk and calcium nitrate with the purpose of achieving highly stable CaO precursors for thermochemical energy storage (TCES) of concentrated solar power (CSP) via the Calcium Looping (CaL) process. CaL conditions for CSP storage would involve carbonation under high CO_2 partial pressure at high temperature and calcination at moderate temperature. Such conditions promote CaO pore-plugging, which hinders the multicycle activity of limestone derived CaO for particles sufficiently large to be employed in practice. The use of nanosilica as a biotemplate serves to enhance CaO thermal stability while at the same time is useful to avoid pore-plugging effects as demonstrated on the present work. The composites synthesized with 70% and 90% CaO load, respectively, preserve the morphology of rice husk. Both composites exhibit a notably enhanced effective conversion (which takes into account the presence of inert SiO_2) as compared to limestone with particles larger than 45 μm. Our study shows that pore-plugging is mitigated by the porous structure and uniform CaO/SiO_2 dispersion obtained from the biotemplate synthesis method leading to high values of the multicycle conversion for large enough particles to be captured in cyclonic separators employed in practice.

Acknowledgments

This work has been supported by the Spanish Government Agency Ministerio de Economia y Competitividad (MINECO-FEDER funds, contracts CTQ2014-52763-C2, CTQ2017-83602-C2). The authors sincerely acknowledge Herba Ricemills, Omya Clariana and Segura S.L. companies for supplying the materials used in the present study. AP thanks financial

support from VI PPIT-US and VPPI-US for his current contract. We acknowledge the Functional Characterization and Microscopy services of the Innovation, Technology and Research Center of the University of Seville (CITIUS) and the Characterization services of the Institute of Materials Science of Seville (ICMS).

References

[1] Blamey J, Anthony EJ, Wang J, Fennell PS. The calcium looping cycle for large-scale CO_2 capture. Progress in Energy and Combustion Science 2010;36(2):260-79.

[2] Kierzkowska AM, Pacciani R, Müller CR. CaO-Based CO_2 Sorbents: From Fundamentals to the Development of New, Highly Effective Materials. ChemSusChem 2013;6(7):1130-48.

[3] Valverde JM. Ca-based synthetic materials with enhanced CO_2 capture efficiency. Journal of Materials Chemistry A 2013;1(3):447-68.

[4] Shimizu T, Hirama T, Hosoda H, Kitano K, Inagaki M, Tejima K. A Twin Fluid-Bed Reactor for Removal of CO_2 from Combustion Processes. Chemical Engineering Research and Design 1999;77(1):62-8.

[5] Barker R. The reactivity of calcium oxide towards carbon dioxide and its use for energy storage. Journal of Applied Chemistry and Biotechnology 1974;24(4-5):221-7.

[6] Flamant G, Hernandez D, Bonet C, Traverse J-P. Experimental aspects of the thermochemical conversion of solar energy; Decarbonation of $CaCO_3$. Solar Energy 1980;24(4):385-95.

[7] Peng Q, Yang X, Ding J, Wei X, Yang J. Design of new molten salt thermal energy storage material for solar thermal power plant. Applied Energy 2013;112:682-9.

[8] Fernández AG, Ushak S, Galleguillos H, Pérez FJ. Development of new molten salts with $LiNO_3$ and $Ca(NO_3)_2$ for energy storage in CSP plants. Applied Energy 2014;119:131-40.

[9] Vignarooban K, Xu X, Arvay A, Hsu K, Kannan AM. Heat transfer fluids for concentrating solar power systems – A review. Applied Energy 2015;146:383-96.

[10] Zhao B-c, Cheng M-s, Liu C, Dai Z-m. Cyclic thermal characterization of a molten-salt packed-bed thermal energy storage for concentrating solar power. Applied Energy 2017;195:761-73.

[11] Albrecht KJ, Jackson GS, Braun RJ. Thermodynamically consistent modeling of redox-stable perovskite oxides for thermochemical energy conversion and storage. Applied Energy 2016;165:285-96.

[12] Cabeza LF, Solé A, Fontanet X, Barreneche C, Jové A, Gallas M, et al. Thermochemical energy storage by consecutive reactions for higher efficient concentrated solar power plants (CSP): Proof of concept. Applied Energy 2017;185, Part 1:836-45.

[13] Tescari S, Singh A, Agrafiotis C, de Oliveira L, Breuer S, Schlögl-Knothe B, et al. Experimental evaluation of a pilot-scale thermochemical storage system for a concentrated solar power plant. Applied Energy 2017;189:66-75.

[14] Chacartegui R, Alovisio A, Ortiz C, Valverde JM, Verda V, Becerra JA. Thermochemical energy storage of concentrated solar power by integration of the calcium looping process and a CO_2 power cycle. Applied Energy 2016;173:589-605.

[15] Erans M, Manovic V, Anthony EJ. Calcium looping sorbents for CO_2 capture. Applied Energy 2016;180:722-42.

[16] Stanmore BR, Gilot P. Review—calcination and carbonation of limestone during thermal cycling for CO_2 sequestration. Fuel Processing Technology 2005;86(16):1707-43.

[17] Valverde JM, Barea-López M, Perejón A, Sanchez-Jimenez PE, Perez-Maqueda LA. Thermochemical Energy Storage for Concentrated Solar Power using natural limestone: Thermal pretreatment and nanosilica addition. Energy & Fuels 2017.

[18] Benitez-Guerrero M, Sarrion B, Perejon A, Sanchez-Jimenez PE, Perez-Maqueda LA, Valverde JM. Large-scale high-temperature solar energy storage using natural minerals. Solar Energy Materials and Solar Cells 2017;168:14-21.

[19] Albrecht KO, Wagenbach KS, Satrio JA, Shanks BH, Wheelock TD. Development of a CaO-Based CO_2 Sorbent with Improved Cyclic Stability. Industrial & Engineering Chemistry Research 2008;47(20):7841-8.
[20] Li L, King DL, Nie Z, Howard C. Magnesia-Stabilized Calcium Oxide Absorbents with Improved Durability for High Temperature CO_2 Capture. Industrial & Engineering Chemistry Research 2009;48(23):10604-13.
[21] Broda M, Kierzkowska AM, Müller CR. Influence of the Calcination and Carbonation Conditions on the CO_2 Uptake of Synthetic Ca-Based CO_2 Sorbents. Environmental Science & Technology 2012;46(19):10849-56.
[22] Radfarnia HR, Iliuta MC. Development of Zirconium-Stabilized Calcium Oxide Absorbent for Cyclic High-Temperature CO_2 Capture. Industrial & Engineering Chemistry Research 2012;51(31):10390-8.
[23] Vieille L, Govin A, Grosseau P. Improvements of calcium oxide based sorbents for multiple CO_2 capture cycles. Powder Technology 2012;228:319-23.
[24] Antzara A, Heracleous E, Lemonidou AA. Improving the stability of synthetic CaO-based CO_2 sorbents by structural promoters. Applied Energy 2015;156:331-43.
[25] Chen H, Zhang P, Duan Y, Zhao C. Reactivity enhancement of calcium based sorbents by doped with metal oxides through the sol–gel process. Applied Energy 2016;162:390-400.
[26] Ortiz C, Valverde JM, Chacartegui R, Benítez-Guerrero M, Perejón A, Romeo LM. The Oxy-CaL process: A novel CO_2 capture system by integrating partial oxy-combustion with the Calcium-Looping process. Applied Energy 2017;196:1-17.
[27] Romeo LM, Lara Y, Lisbona P, Martínez A. Economical assessment of competitive enhanced limestones for CO_2 capture cycles in power plants. Fuel Processing Technology 2009;90(6):803-11.
[28] Huang C-H, Chang K-P, Yu C-T, Chiang P-C, Wang C-F. Development of high-temperature CO_2 sorbents made of CaO-based mesoporous silica. Chemical Engineering Journal 2010;161(1–2):129-35.
[29] Valverde JM, Perejon A, Perez-Maqueda LA. Enhancement of fast CO_2 capture by a nano-SiO_2/CaO composite at Ca-looping conditions. Environmental Science and Technology 2012;46(11):6401-8.
[30] Sanchez-Jimenez PE, Perez-Maqueda LA, Valverde JM. Nanosilica supported CaO: A regenerable and mechanically hard CO_2 sorbent at Ca-looping conditions. Applied Energy 2014;118:92-9.
[31] Wang M, Lee C-G, Ryu C-K. CO_2 sorption and desorption efficiency of Ca_2SiO_4. International Journal of Hydrogen Energy 2008;33(21):6368-72.
[32] Li Y, Zhao C, Ren Q, Duan L, Chen H, Chen X. Effect of rice husk ash addition on CO_2 capture behavior of calcium-based sorbent during calcium looping cycle. Fuel Processing Technology 2009;90(6):825-34.
[33] Chen H, Zhao C, Ren Q. Feasibility of CO_2/SO_2 uptake enhancement of calcined limestone modified with rice husk ash during pressurized carbonation. Journal of Environmental Management 2012;93(1):235-44.
[34] Sun J, Liu W, Hu Y, Li M, Yang X, Zhang Y, et al. Structurally Improved, Core-in-Shell, CaO-Based Sorbent Pellets for CO<inf>2</inf> Capture. Energy and Fuels 2015;29(10):6636-44.
[35] Sun J, Liu W, Wang W, Hu Y, Yang X, Chen H, et al. CO_2 Sorption Enhancement of Extruded-Spheronized CaO-Based Pellets by Sacrificial Biomass Templating Technique. Energy & Fuels 2016;30(11):9605-12.
[36] ISO 14887: Sample preparation—Dispersing procedures for particles in liquids. In: ISO, ed.: Genève 2000.
[37] Brunauer S, Emmett PH, Teller E. Adsorption of Gases in Multimolecular Layers. Journal of the American Chemical Society 1938;60(2):309-19.

[38] Barrett EP, Joyner LG, Halenda PP. The Determination of Pore Volume and Area Distributions in Porous Substances. I. Computations from Nitrogen Isotherms. Journal of the American Chemical Society 1951;73(1):373-80.
[39] Ortiz C, Chacartegui R, Valverde JM, Becerra JA, Perez-Maqueda LA. A new model of the carbonator reactor in the calcium looping technology for post-combustion CO_2 capture. Fuel 2015;160:328-38.
[40] Real C, Alcalá MD, Criado JM. Preparation of Silica from Rice Husks. Journal of the American Ceramic Society 1996;79(8):2012-6.
[41] Kalapathy U, Proctor A, Shultz J. A simple method for production of pure silica from rice hull ash. Bioresource Technology 2000;73(3):257-62.
[42] Della VP, Kühn I, Hotza D. Rice husk ash as an alternate source for active silica production. Materials Letters 2002;57(4):818-21.
[43] Wang W, Martin JC, Fan X, Han A, Luo Z, Sun L. Silica Nanoparticles and Frameworks from Rice Husk Biomass. ACS Applied Materials & Interfaces 2012;4(2):977-81.
[44] Ettarh C, Galwey AK. A kinetic and mechanistic study of the thermal decomposition of calcium nitrate. Thermochimica Acta 1996;288(1):203-19.
[45] Krishnarao RV, Godkhindi MM. Distribution of silica in rice husks and its effect on the formation of silicon carbide. Ceramics International 1992;18(4):243-9.
[46] Barker R. The reversibility of the reaction $CaCO_3 \rightleftarrows CaO+CO_2$. Journal of Applied Chemistry and Biotechnology 1973;23(10):733-42.
[47] Grasa G, Murillo R, Alonso M, Abanades JC. Application of the random pore model to the carbonation cyclic reaction. AIChE Journal 2009;55(5):1246-55.
[48] Bhatia SK, Perlmutter DD. Effect of the product layer on the kinetics of the CO_2-lime reaction. AIChE Journal 1983;29(1):79-86.
[49] Sun Z, Luo S, Qi P, Fan L-S. Ionic diffusion through Calcite ($CaCO_3$) layer during the reaction of CaO and CO_2. Chemical Engineering Science 2012;81:164-8.
[50] Sarrion B, Valverde JM, Perejon A, Perez-Maqueda L, Sanchez-Jimenez PE. On the multicycle activity of natural limestone/dolomite for thermochemical energy storage of concentrated solar power. Energy Technology 2016;4(8):1013-9.
[51] Pardo P, Deydier A, Anxionnaz-Minvielle Z, Rougé S, Cabassud M, Cognet P. A review on high temperature thermochemical heat energy storage. Renewable and Sustainable Energy Reviews 2014;32:591-610.
[52] Green DW, Perry RH. Perry's Chemical Engineers' Handbook. 8th ed.: Mc Graw-Hill; 2007.

Figures

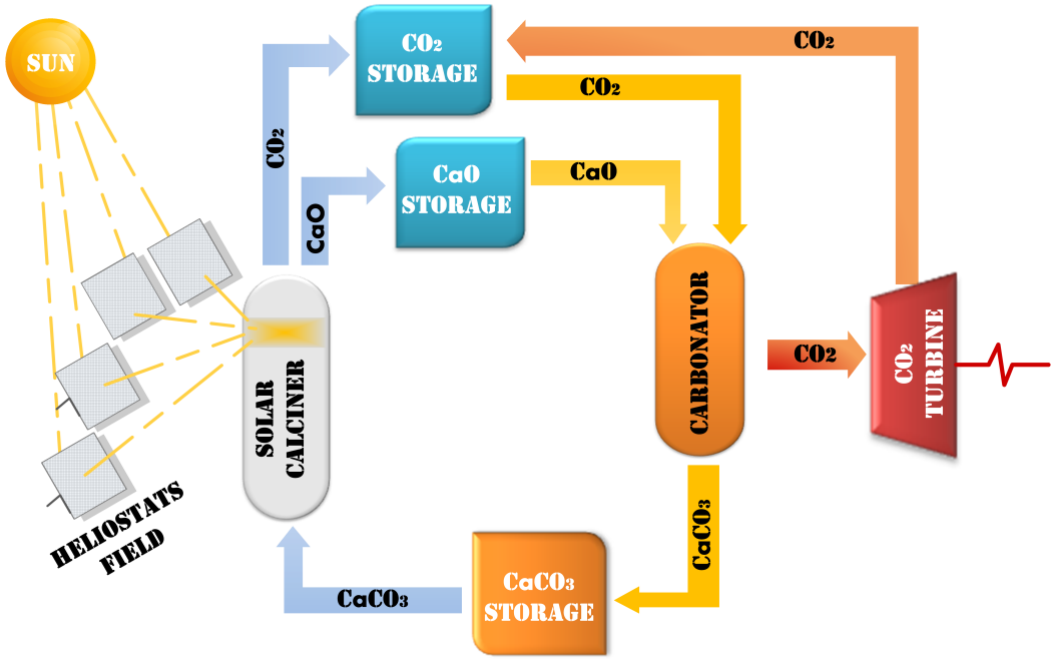

Fig. 1. Flow diagram of the Calcium-Looping thermochemical energy storage system for CSP plants. A detailed energy integration scheme is found in Ref. [14].

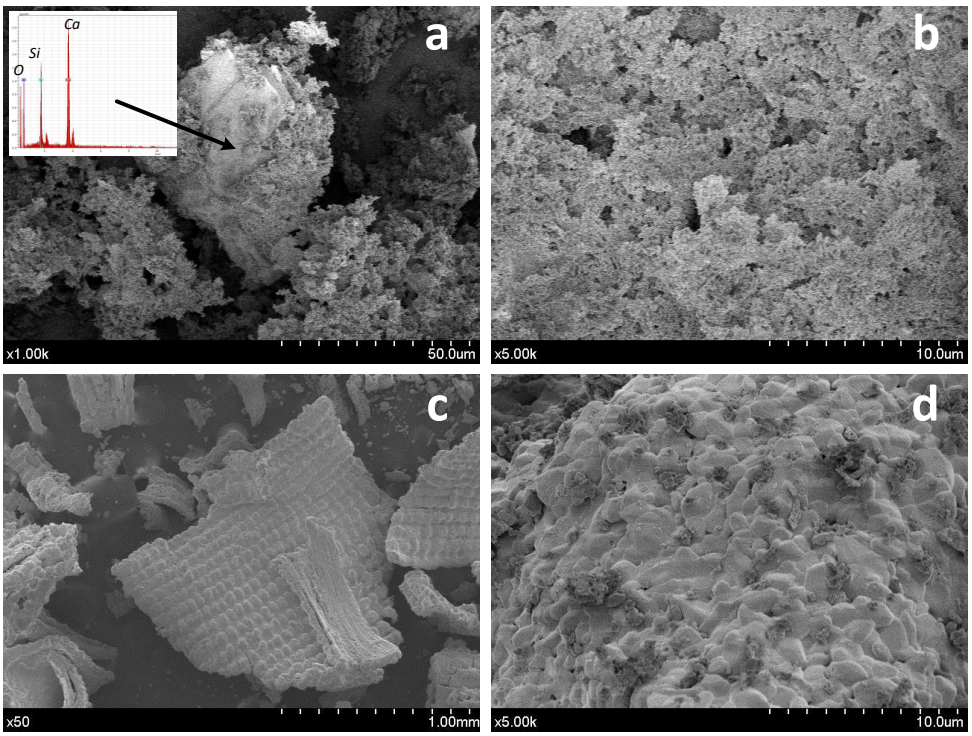

Fig. 2. SEM micrographs of as-prepared 70%CaO composite (a, b) and 90%CaO composite (c, d).

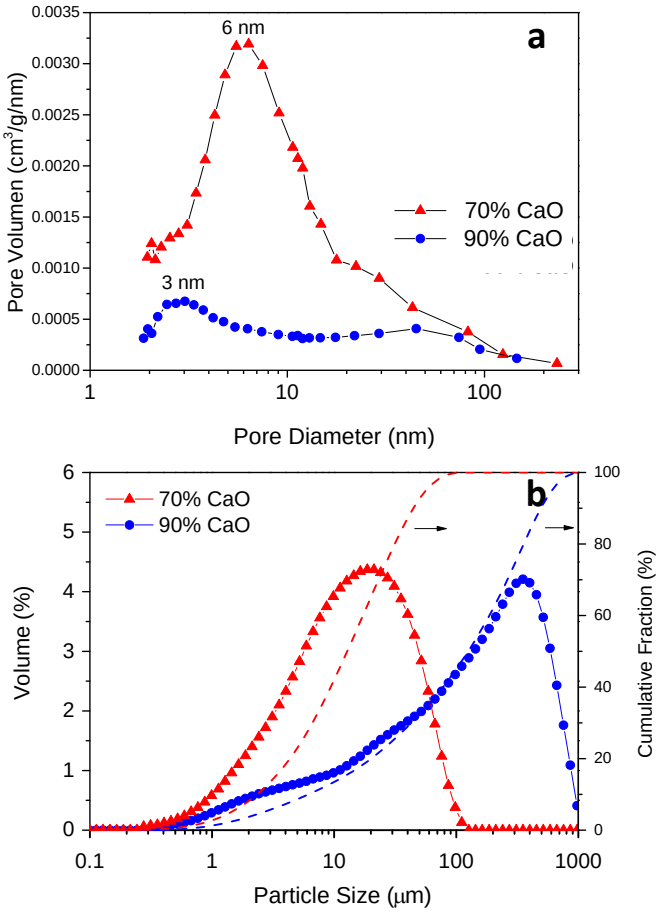

Fig. 3. Pore size distribution (BJH) (a) and particle size frequency and cumulative distributions (b) measured for as-prepared composite materials.

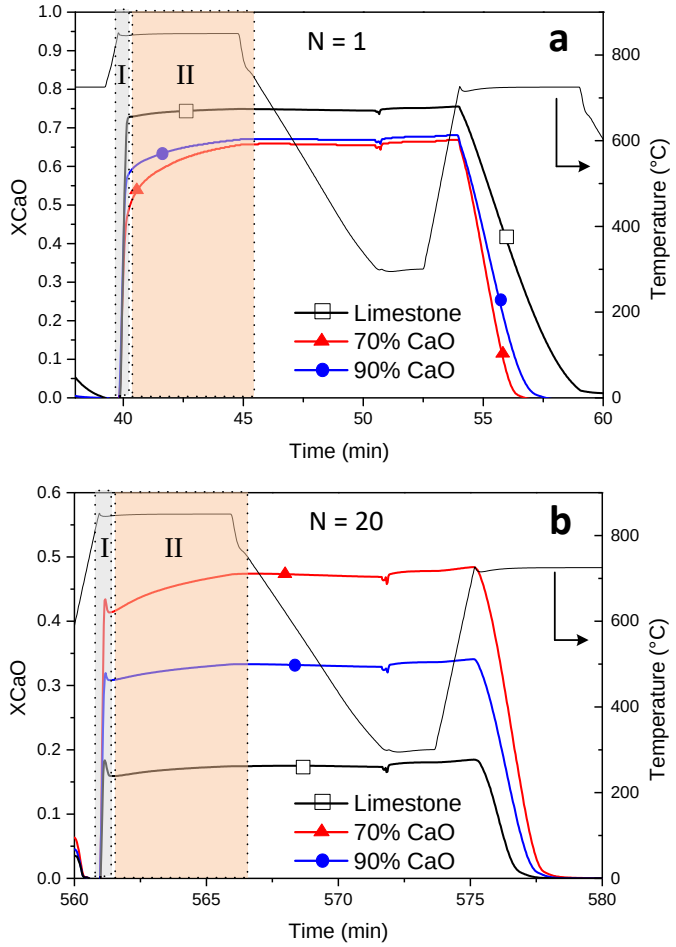

Fig. 4. Time evolution of CaO conversion and temperature during 1st (a) and 20th (b) cycles for the CaO/SiO_2 composites tested under CaL-CSP storage conditions. Colored regions I and II correspond to fast reaction and slow solid-state diffusion controlled phases respectively.

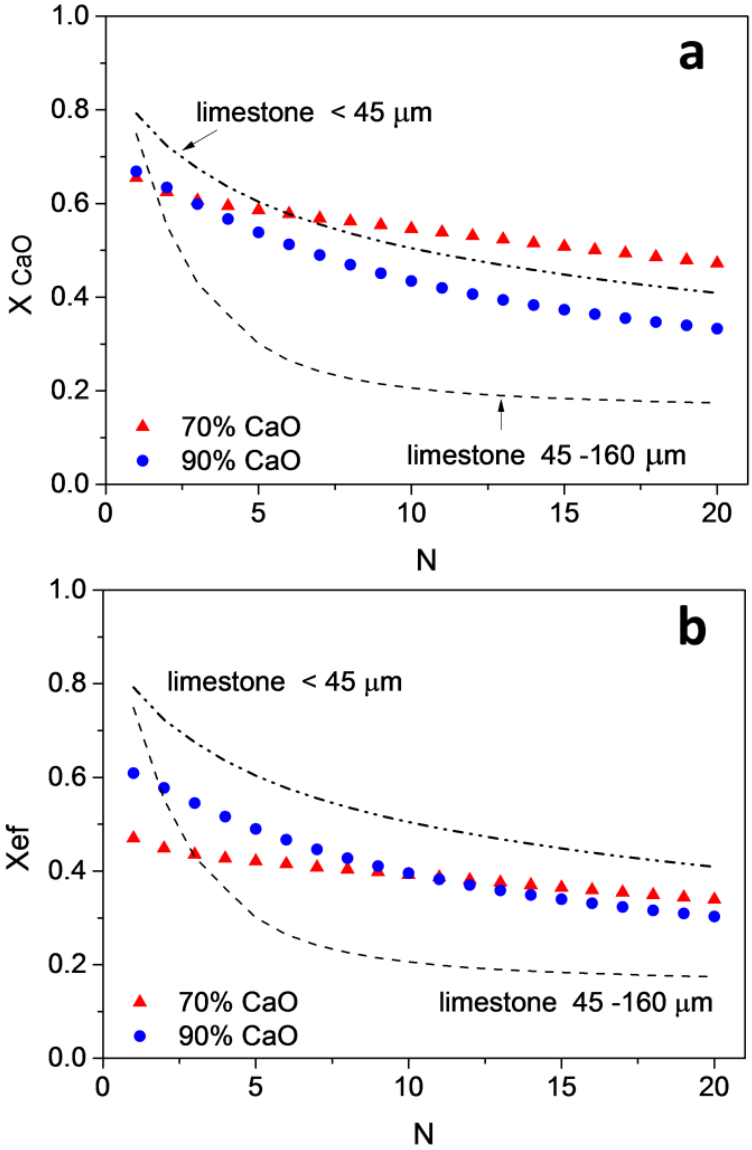

Fig. 5. CaO conversion (a) and effective conversion (b) at the end of the carbonation stage as a function of the cycle number for the CaO/SiO_2 composites tested under CaL-CSP storage conditions. Multicycle conversion data for sieved limestone samples reported elsewhere are plotted for comparison

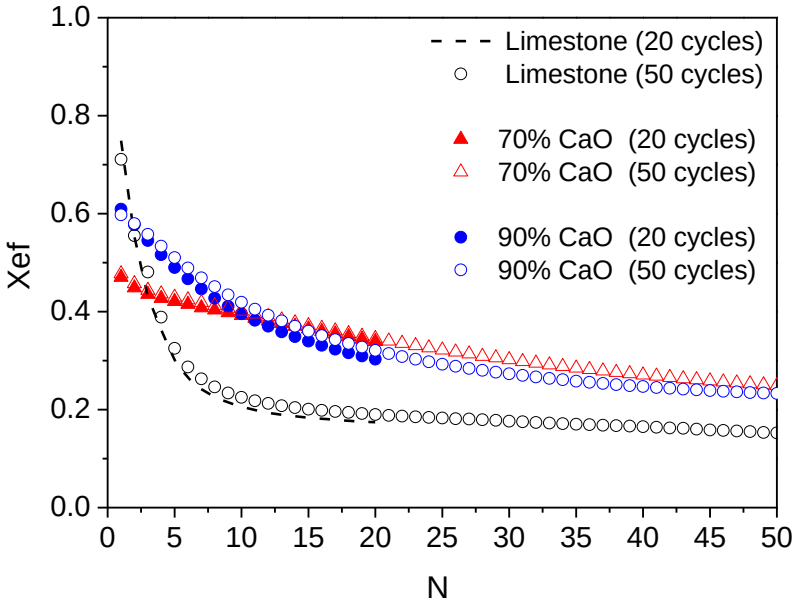

Fig. 6. Effective conversion as a function of the cycle number for both synthetic composites and limestone samples of similar particle size tested under CaL-CSP storage conditions for 20 and 50 cycles.

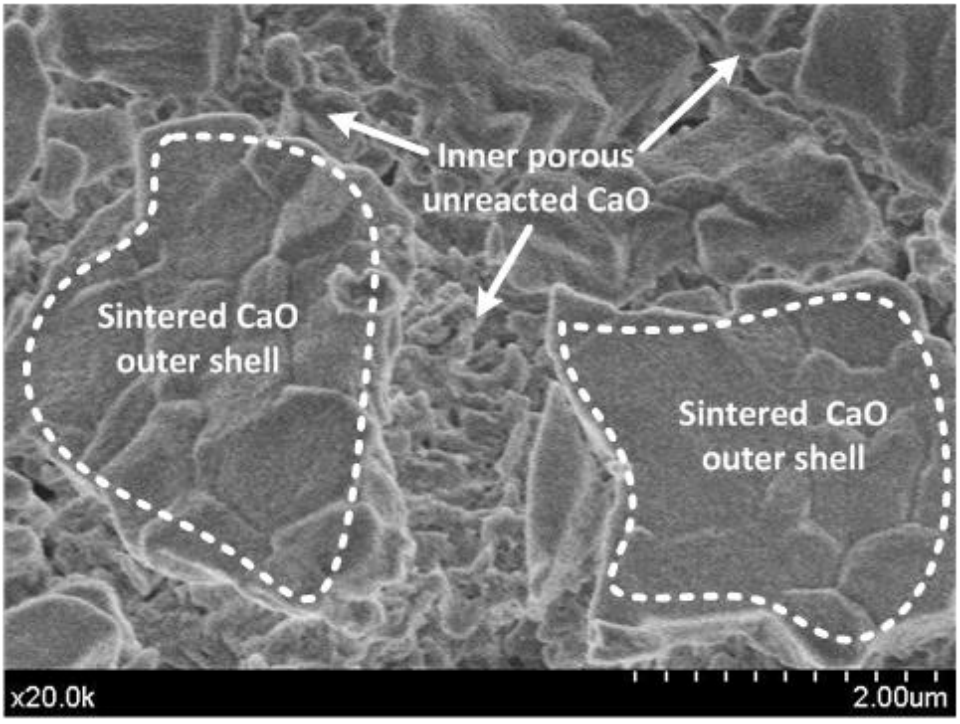

Fig. 7. SEM picture of a limestone sample after 20 CaL cycles ending in calcination and with a broken surface that illustrates a porous inner CaO skeleton onto which a CaO sintered layer is formed.

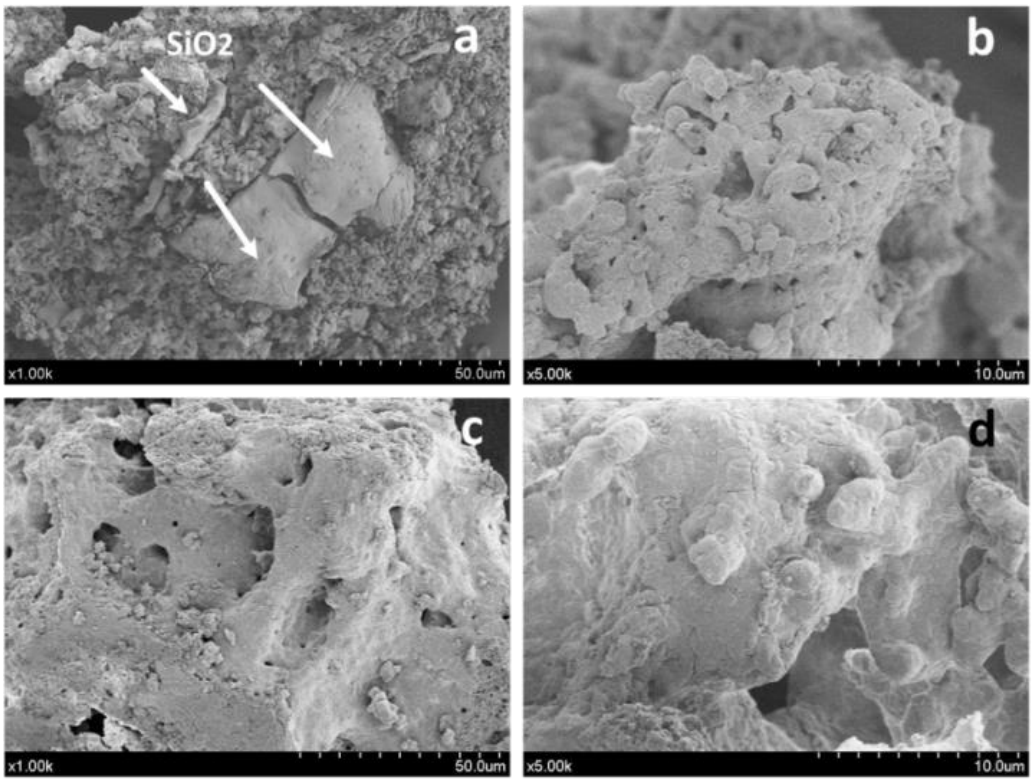

Fig. 8. SEM micrographs of 70%CaO (a, b) and 90%CaO (c, d) composites after 20 CaL cycles.

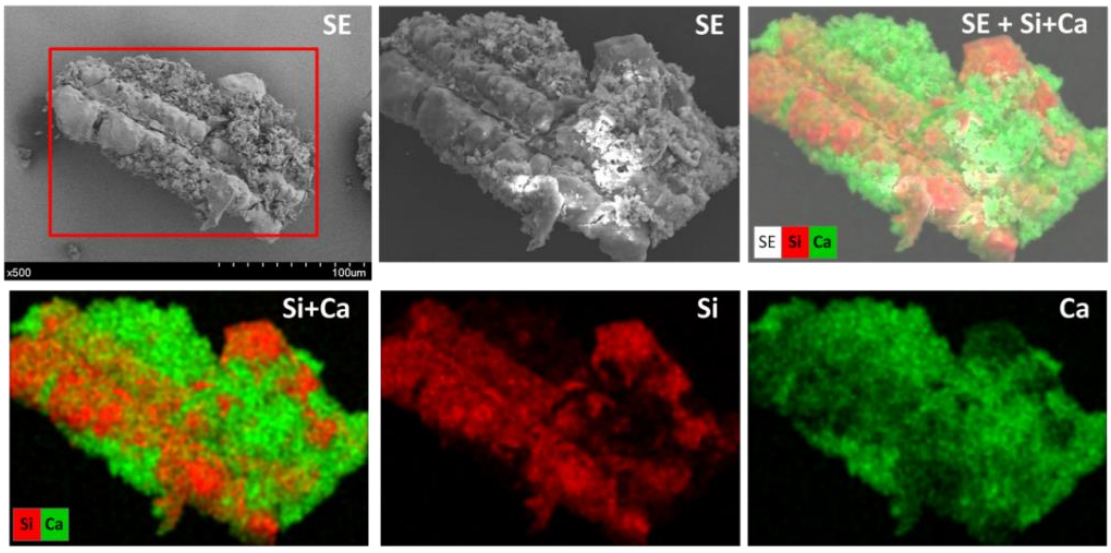

Fig. 9. Secondary electron micrographs (SE at 2 and 20 kV) and compositional mapping (Ca and Si) of the 70%CaO composite sample after 20 CaL cycles.

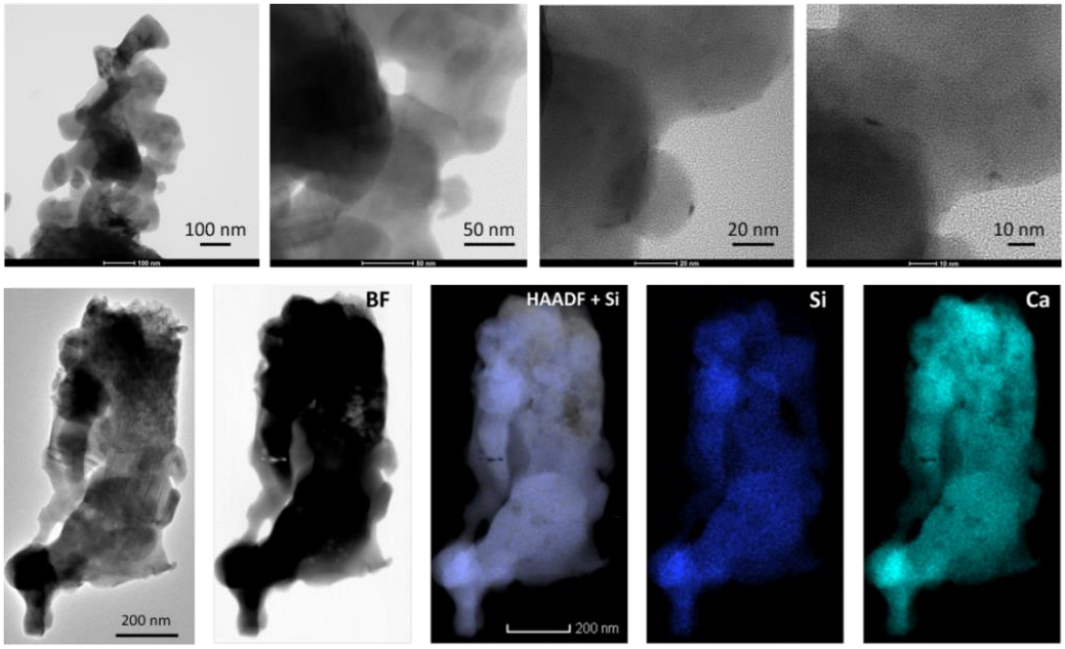

Fig. 10. HRTEM micrographs and HAADF-STEM mapping for Si and Ca elements of 70%CaO composite after being subjected to 20 cycles under CaL-CSP conditions.

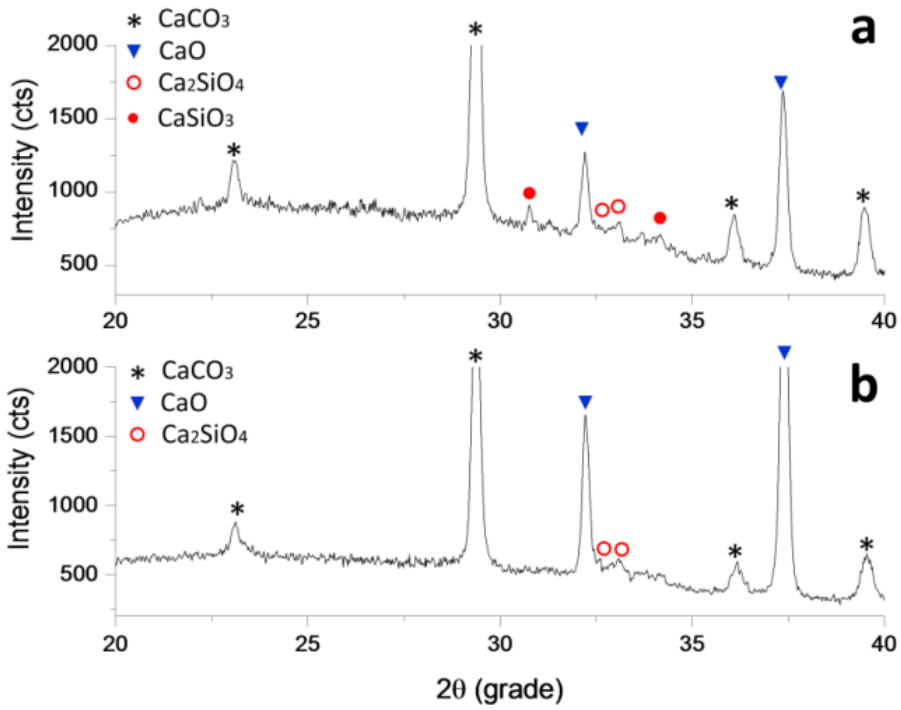

Fig. 11. XRD patterns recorded for the 70%CaO (a) and 90%CaO (b) samples after being cycled.

Appendix (Supplementary Content):

Pretreatment of Rice Husk and Synthesis of Rice Husk Ash

In our work raw rice husk was pretreated to be used as template. First, rice husk was ground to 1 mm (centrifugal blade-mill, Retsch ZM1). Afterwards, the milled husk was washed in distilled boiling water for 2 hours. The washing process was repeated twice after water replacement. Finally, the husk was oven-dried at 120 ºC. SEM micrographs of pretreated rice husk are shown in Fig. A3. This pretreatment ensures the removal of alkali elements [35], and the obtention of high purity nanostructured SiO_2 of large specific surface area.

In order to characterize and quantify the ash content, pretreated rice husk was thermally treated. Rice husk ash was obtained following two steps thermal treatment in which pyrolysis and combustion take place separately to attain large surface area. A first pyrolysis stage was carried out under nitrogen atmosphere at a heating rate of 3 ºC min^{-1} from ambient temperature to 600 ºC, which was kept for 3 h. This produces an amorphous carbon skeleton and inorganic ash. The second stage consists of combustion at 600 ºC under air for 3 h to remove the carbonaceous char as was inferred from TG/DSC observations (Fig. A4). A quantity of 1.5 g of pretreated rice husk was subjected to this thermal treatment in a tubular oven using a flow rate of 100 $mLmin^{-1}$. The weight of the residual inorganic ash obtained corresponds to 11% of the initial raw sample weight (mean value from three independent runs). Composition, microstructure and specific surface area of the synthesized rice husk ash were analyzed using XRF, XRD, SEM, HRTEM and N_2 adsorption-desorption isotherms, described in the experimental section.

Additional Figures:

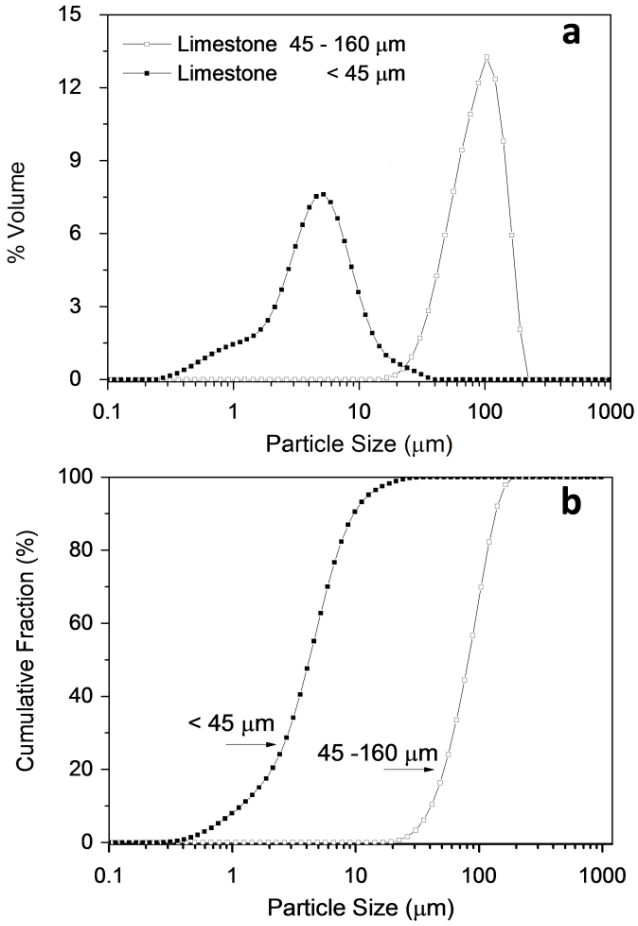

Fig.A1. PSD of limestone samples sieved < 45 microns and 45-160 microns.

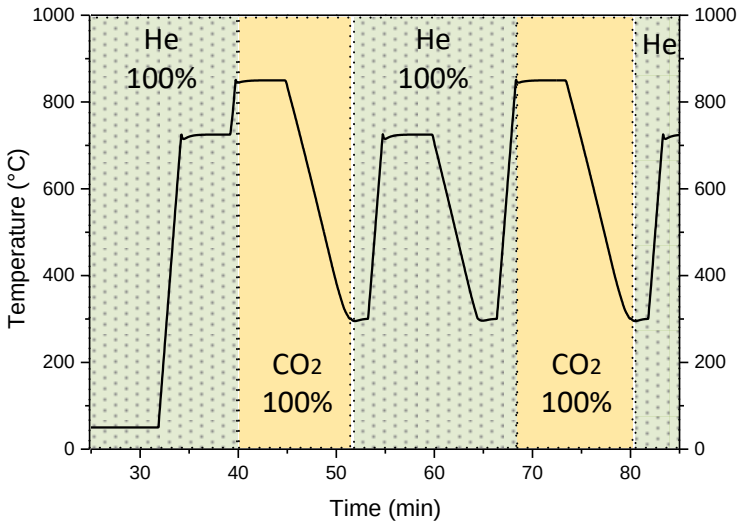

Fig.A2. Schematic representation of the temperature program carried out to test the multicycle performance of the synthesized CaO-SiO_2 composites under CaL-CSP conditions using a Q5000IR thermogravimetric analyzer (TA Instruments). The colored regions indicate the gas atmosphere employed in each calcination/carbonation step.

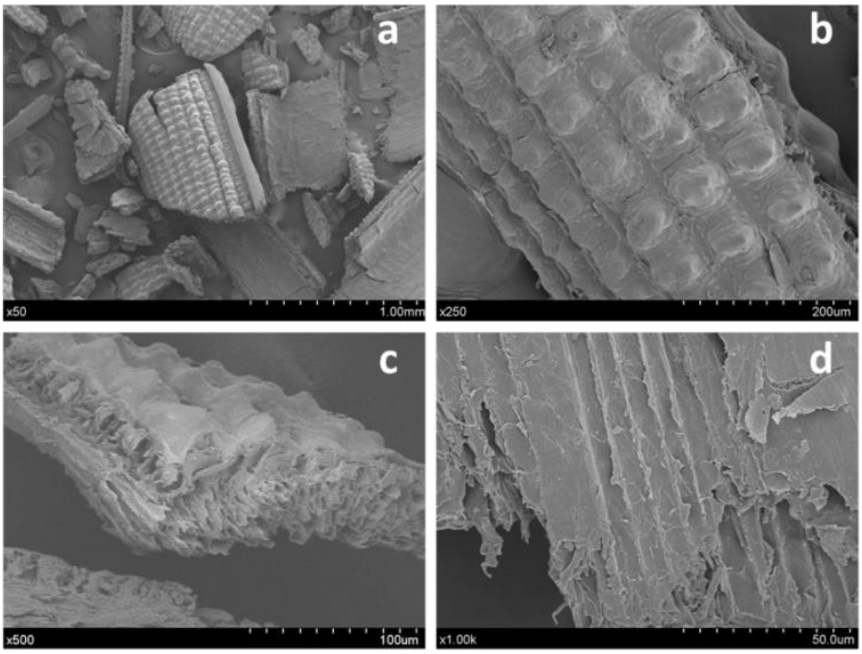

Fig. A3. SEM micrographs of the biotemplate prepared in this work by milling, hot-washing and drying rice husk as detailed in the experimental section.

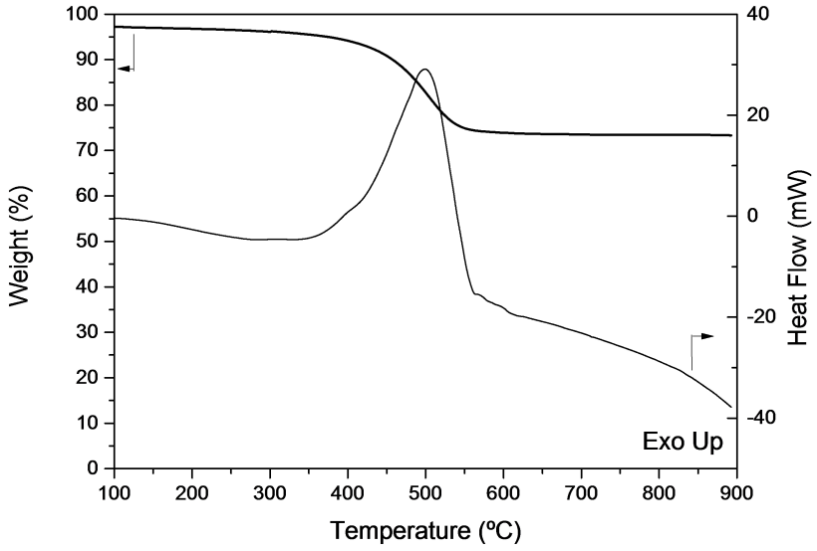

Fig. A4. Thermogravimetry and differential scanning calorimetry of pre-pyrolyzed rice husk under TG/DSC was conducted using a SDT Q600 (TA Instruments) in the temperature range 25-900 ºC and using a heating ramp of 10 ºC min^{-1} under an air flow rate of 100 mL min^{-1}. 10 mg sample was employed.

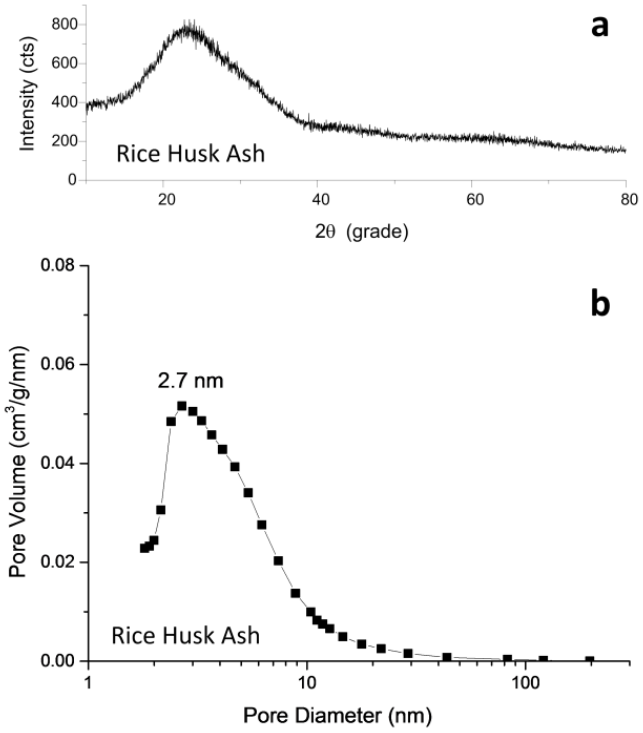

Fig.A5. Powder X-Ray diffractogram (a) and BJH pore size distribution (b) of rice husk ash.

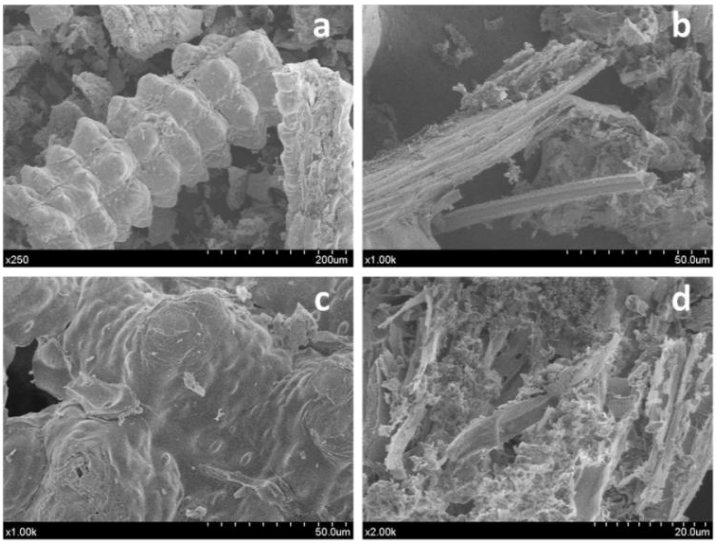

Fig. A6. SEM micrographs of rice husk ash

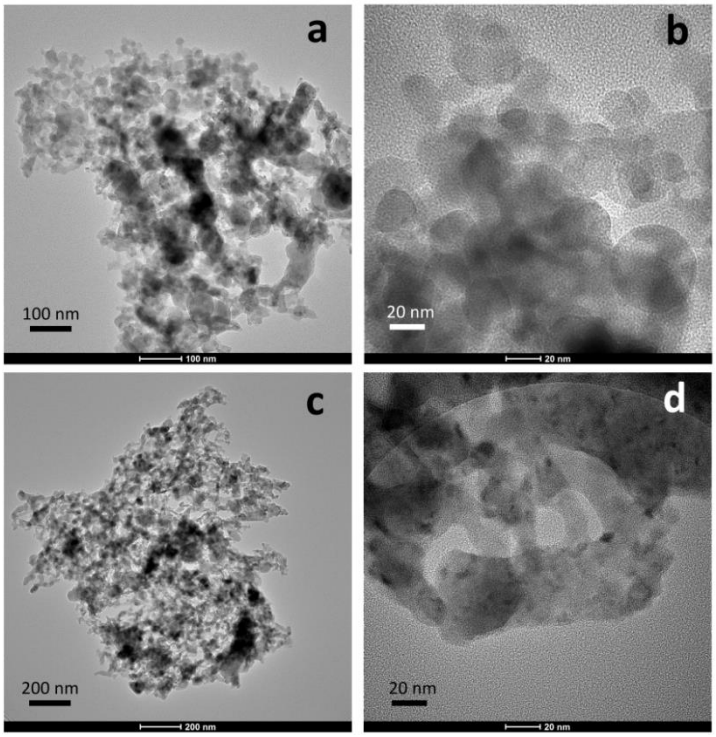

Fig. A7. TEM micrographs of rice husk ash

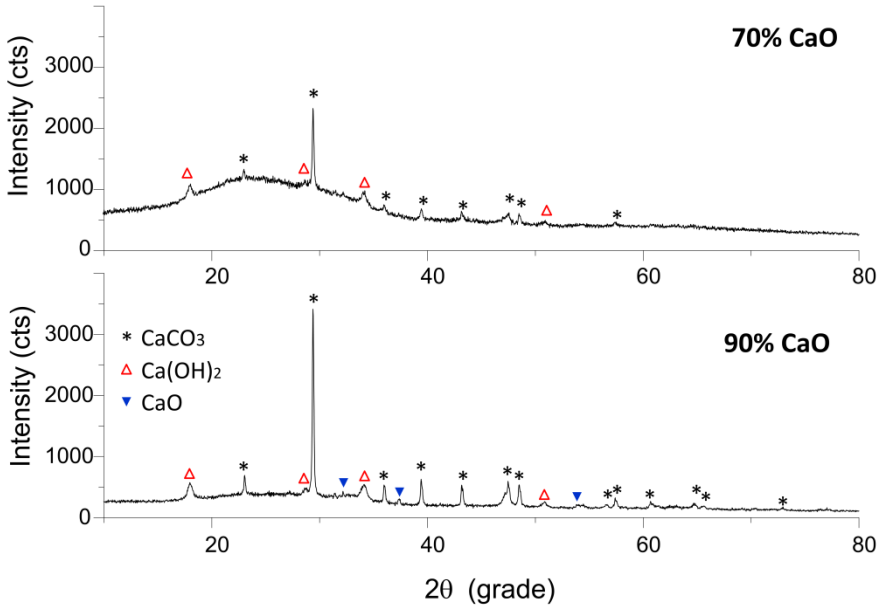

Fig. A8. Powder X-ray diffractograms of as-prepared composites with different CaO loads.

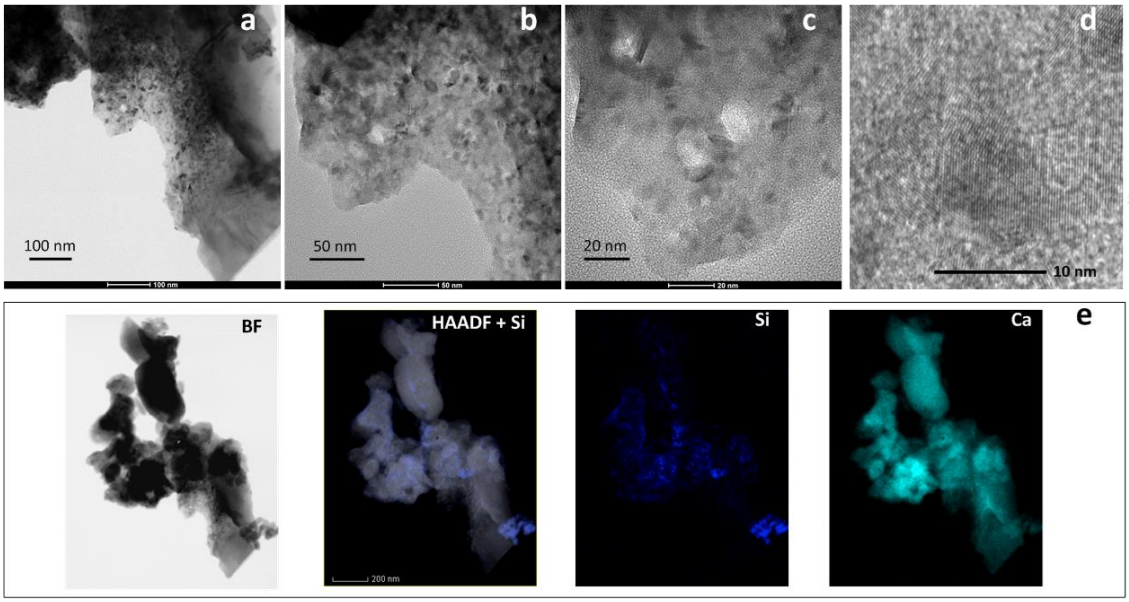

Fig. A9. HRTEM micrographs (a-d) and HAADF-STEM mapping for Si and Ca elements (e) of as-prepared 70%CaO composite.

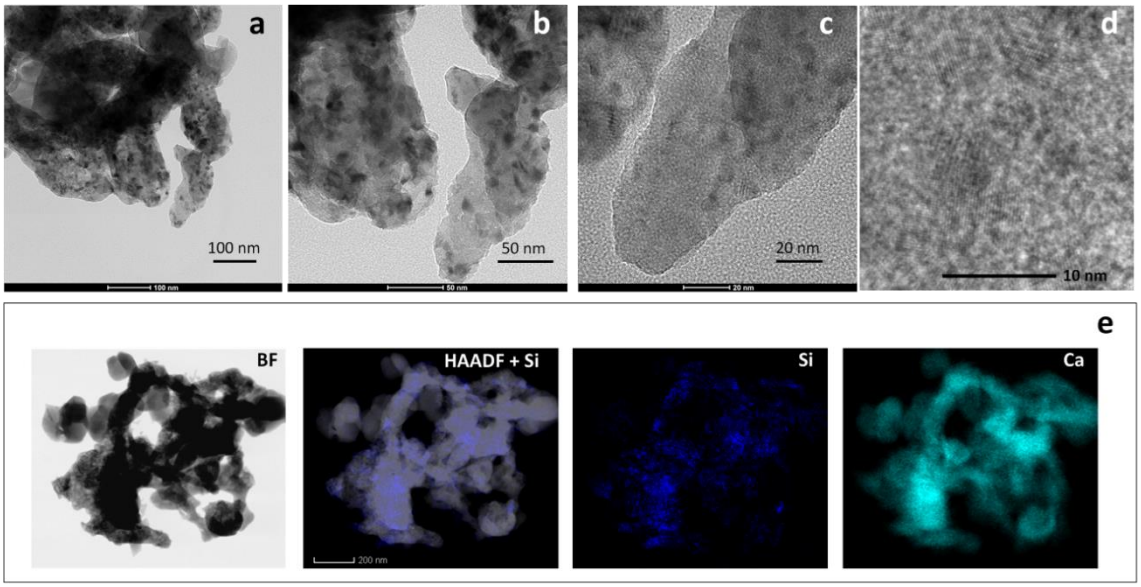

Fig.A10. HRTEM micrographs (a-d) and HAADF-STEM mapping for Si and Ca elements (e) of as-prepared 90%CaO composite.

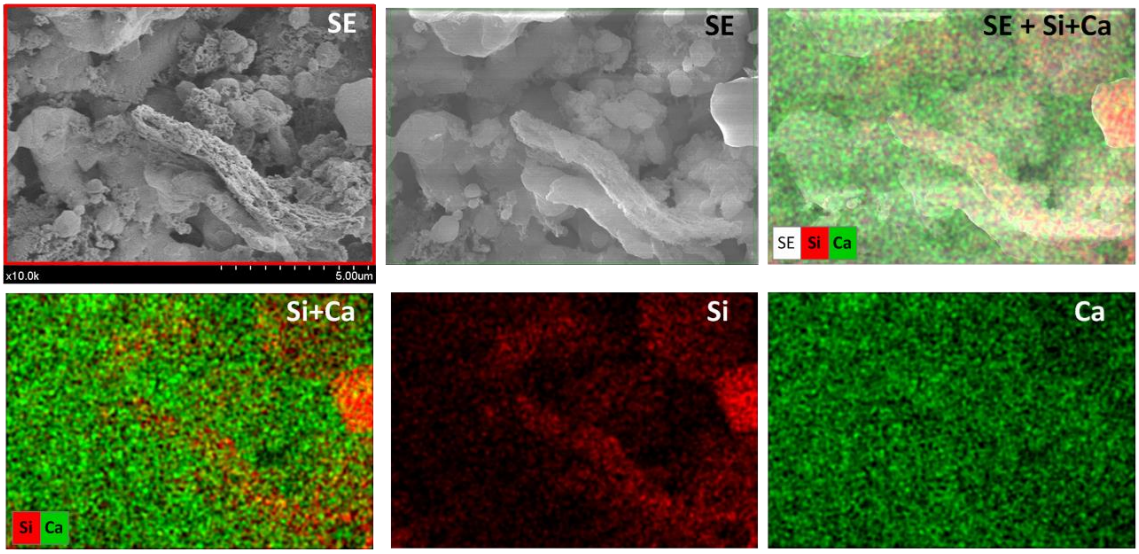

Fig.A11. Secondary electron micrographs (SE at 2 and 20kV) and compositional mapping (Ca and Si) of 70%CaO composite after being subjected to 20 cycles under CaL-CSP conditions.

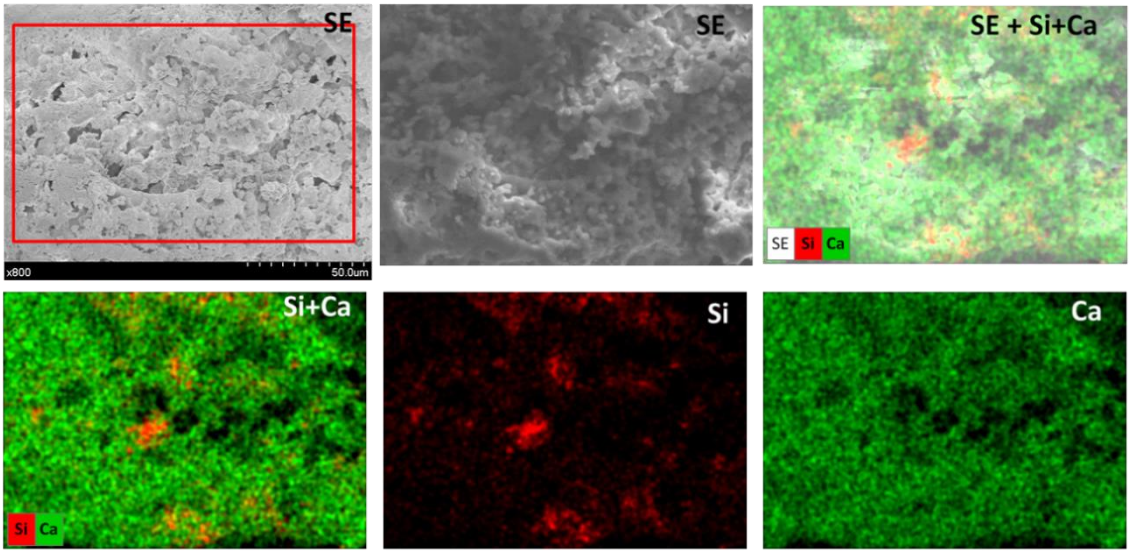

Fig.A12. Secondary electron micrographs (SE at 2 and 20kV) and compositional mapping (Ca and Si) of 90%CaO composite after being subjected to 20 cycles under CaL-CSP conditions.

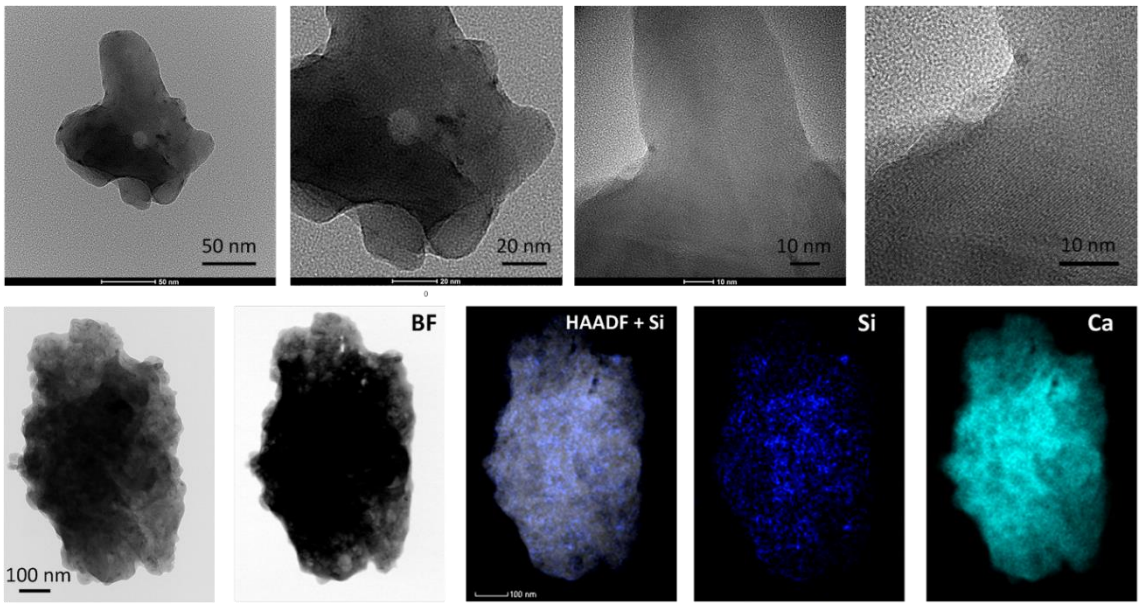

Fig. A13. HRTEM micrographs and HAADF-STEM mapping for Si and Ca elements of the 90%CaO composite sample after 20 cycles.